INSTITUTE OF PHYSICS PUBLISHING JOURNAL OF PHYSICS B: ATOMIC, MOLECULAR AND OPTICAL PHYSICS

J. Phys. B: At. Mol. Opt. Phys. **38** (2005) 2965–2977 doi:10.1088/0953-4075/38/16/009

Low energy (e, 2e) differential cross-section measurements on the $1\pi_g$ and $4\sigma_g$ molecular orbitals of CO_2

Martyn J Hussey and Andrew J Murray

School of Physics and Astronomy, Schuster Laboratory, The University of Manchester, Manchester, M13 9PL, UK

E-mail: Andrew.Murray@manchester.ac.uk

Received 14 April 2005, in final form 29 May 2005
Published 3 August 2005
Online at stacks.iop.org/JPhysB/38/2965

Abstract

Ionization differential cross sections are presented for low energy electron scattering from the $1\pi_g$ and $4\sigma_g$ orbitals of the tri-atomic molecule CO_2, at incident electron energies ranging from 10 eV to 80 eV above the ionization threshold. The (e, 2e) experiments were conducted in a coplanar symmetric geometry, the outgoing electrons sharing the excess energy from the interaction equally. The results are compared to experiments previously conducted in the same geometry and over the same energy range from the $1\pi_u$ and $3\sigma_g$ orbitals of N_2. An unusual feature has been discovered ionizing from the $1\pi_g$ orbital at a scattered and ejected electron energy of 10 eV, where a second forward scattering peak is found at low angles.

1. Introduction

Understanding ionization of atoms and molecules by low energy electrons remains one of the most difficult problems facing atomic and molecular physics. The greatest detail is obtained when angular correlations are measured between 'scattered' and 'ejected' electrons following ionization by an incident electron, commonly referred to as an (e, 2e) experiment. Selection of different momenta for the outgoing electrons allows a complete description of the ionization process to be obtained, with experiments typically ranging in energy from a few eV to several thousands eV above the ionization threshold [1]. In the low energy region from threshold to around 100 eV, ionization is highly sensitive to different processes such as post-collisional interactions, polarization of the target, interference effects between the outgoing electrons and multiple collisions [2–6]. In this energy regime all of these processes have comparable importance, and so accurate modelling of the reaction is extremely challenging.

The (e, 2e) process may be represented by the reaction:

$$e_0(E_0, \mathbf{k}_0) + A \rightarrow A^+ + e_a(E_a, \mathbf{k}_a) + e_b(E_b, \mathbf{k}_b), \quad (1)$$

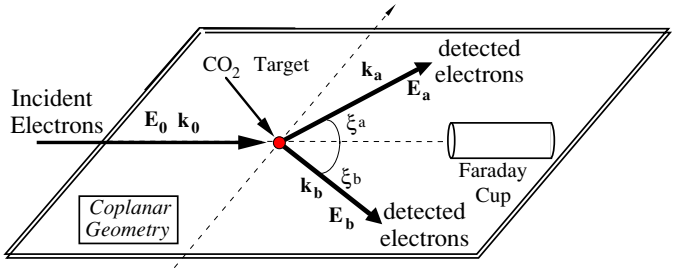

Figure 1. The (e, 2e) spectrometer configured in a coplanar geometry. The experiment is carried out in a symmetric geometry, where $\xi_a = \xi_b = \xi$ and $E_a = E_b$.

where e_0 represents the incident electron with energy E_0 and momentum $\mathbf{k}_0$, A and A^+ correspond to the target before and after ionization, and e_a, e_b denote the electrons emerging from the reaction with energies E_a, E_b and momenta $\mathbf{k}_a$, $\mathbf{k}_b$, respectively. In the experiments reported here, the spin of the electrons is not measured, reducing the kinematical constraints to energy and momentum conservation. The outgoing electrons may have a range of different momenta, and so ionization can be described for a given incident energy E_0 by a differential cross section (DCS):

$$\mathrm{DCS} = \frac{\mathrm{d}^3\sigma}{\mathrm{d}E_a\,\mathrm{d}\Omega_a\,\mathrm{d}\Omega_b}, \tag{2}$$

where $\mathrm{d}\Omega_a$ and $\mathrm{d}\Omega_b$ are solid angles defining the direction of the outgoing electrons and E_a represents the energy of one of these electrons.

Experimentally it is necessary to restrict the number of variables when determining the DCS by holding one or more parameters constant, while allowing the remaining to vary. In this paper, (e, 2e) differential cross sections are presented for ionization from the $1\pi_g$ and $4\sigma_g$ molecular orbitals of CO_2. The measurements were conducted in a coplanar symmetric geometry, the incident and detected electrons being in the same plane. An additional constraint imposed was that the scattered and ejected electrons were detected at symmetrically equal angles $\xi = \xi_a = \xi_b$ and equal energies $E_a = E_b$ (figure 1). DCS measurements were obtained at impact energies E_0 from 23.8 eV to 99.39 eV, with the scattered and ejected electron energies ranging from 5 eV to 40 eV. This spans the energy range used in the DCS measurements for N_2 presented by Hussey and Murray [7], allowing comparison between the diatomic N_2 molecule and the tri-atomic CO_2 molecule.

As noted in [7], existing (e, 2e) studies on the ionization dynamics of molecules have mostly been conducted in a coplanar *asymmetric* geometry, with incident electron energies $E_0 > 400$ eV. In these asymmetric experiments the scattered electron carries most of the energy from the reaction and is detected at a fixed forward scattering angle ξ_a. Rioual *et al* [8] and Hussey and Murray [7] present the only (e, 2e) measurements on a molecule conducted in a coplanar symmetric geometry. Rioual *et al* [8] determined the DCS for ionization from the $3\sigma_g$ and $1\pi_u$ orbitals of N_2 at incident energies $E_0 = 100$ eV, 200 eV and 400 eV, whereas Hussey and Murray [7] measured the DCS from the same orbitals at incident energies between 25.6 eV and 76.7 eV. The only existing coplanar (e, 2e) studies from *polyatomic* molecules are by Cavanagh and Lohmann [9] from N_2O, Avaldi and Camilloni [10] from C_2H_2 and Milne-Brownlie *et al* [11] from H_2O. All these polyatomic studies were conducted in a coplanar asymmetric geometry, so it is difficult to draw comparisons between the present CO_2 results and these asymmetric studies. A brief overview of some existing experimental and theoretical (e, 2e) studies on the ionization dynamics of molecules is given in [7].

The motivation for the experiments detailed here is to provide new results for low energy ionization of molecules so as to encourage more rigorous theories to be developed. Furthermore, comparison between measurements from the $1\pi_g$ and $4\sigma_g$ orbitals of the linear *tri-atomic* molecule CO_2 and the measurements presented in [7] for ionization from the $3\sigma_g$ and $1\pi_u$ orbitals of the linear *diatomic* molecule N_2 yields new information on the influence of orbital symmetry and parity. New information is also obtained on ionization of a target with three scattering centres, compared to a diatomic molecule with two scattering centres and an atomic target with only one. There is considerable current interest in the possible effects of Young's double slit interference on the ionization DCS from targets with multiple centres, and these results may provide additional data for these effects [12, 13].

Hussey and Murray [7] found that the DCS measurements for N_2 at low electron impact energies were complicated by the presence of auto-ionizing excited states and shape resonances [7, 14]. DCS measurements at low electron impact energies ($E_0 < 100$ eV) conducted in a coplanar symmetric geometry are also sensitive to effects such as post-collision interactions between the outgoing electrons [15–18]. The DCS measurements on the valence and inner-valence states of CO_2 at low impact energy provide further tests for the influence of these processes on the ionization cross sections.

This paper is divided into four sections. Following this introduction the experimental procedure used to establish these results is briefly described. Experimental data from the $1\pi_g$ orbital of CO_2 are then presented and compared to results from the $1\pi_u$ orbital of N_2. An unexpected feature in the forward scattering results for ionization of the $1\pi_g$ orbital of CO_2 with $E_a = E_b = 10$ eV is detailed, with results collected using a smaller angular interval. Results from the $4\pi_g$ orbital are then presented, allowing comparison with ionization from the $3\sigma_g$ orbital of N_2. Since no theoretical model for CO_2 exists at present in this energy region, conclusions about the variations observed in the DCS are based upon the electron density for the different orbitals of CO_2.

2. Experimental procedure

A complete description of the (e, 2e) coincidence spectrometer and timing electronics used in the experiments presented here is given in [2]. The DCS measurements for ionization of CO_2 were collected in a coplanar symmetric geometry, the scattered and ejected electrons being detected with equal angles $\xi_a = \xi_b = \xi$, and with equal energies $E_a = E_b$. Data were collected at incident electron energies of 23.8 eV, 33.8 eV, 43.8 eV, 53.8 eV and 73.8 eV for the $1\pi_g$ orbital and 29.39 eV, 34.39 eV, 39.39 eV, 59.39 eV, 79.39 eV and 99.39 eV for the $4\sigma_g$ orbital. This corresponds to equal scattered and ejected electron energies of 5 eV, 10 eV, 15 eV, 20 eV and 30 eV for the $1\pi_g$ orbital and 5 eV, 7.5 eV, 10 eV, 20 eV, 30 eV and 40 eV for the $4\sigma_g$ orbital. The incident electrons were generated by a thermionic electron source and as such had a FWHM energy spread of ~600 meV. Scattered and ejected electrons were detected using a pair of hemispherical analysers with an energy and angular resolution of ~500 meV and $\pm 3^\circ$, respectively (further details are given in [2]). Data were collected between $\xi = 40^\circ$ and $\xi = 125^\circ$ for the majority of results presented here. This reduced angular range of the spectrometer compared to the experiments carried out in [7] ($\xi = 35^\circ$ to $\xi = 125^\circ$) was due to a time-of-flight mass spectrometer (TOFMS) being installed to measure fragmentation of the target in a separate series of experiments. The time of flight tube was removed for measurements from the $1\pi_g$ orbital at $E_a = E_b = 10$ eV, with forward scattering measurements being extended to $\xi = 31^\circ$ at this energy.

The CO_2 gas was introduced into the vacuum chamber through a 20 mm long platinum iridium hypodermic needle with internal diameter 0.5 mm via a Negretti needle valve. During

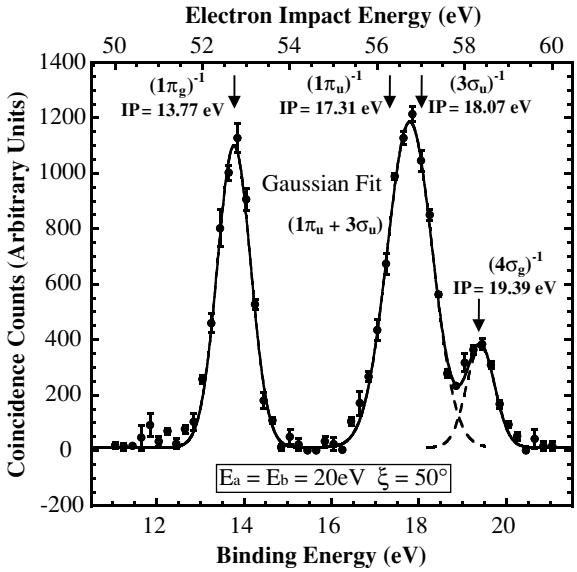

Figure 2. Coincidence energy spectrum for CO_2, showing the binding energy of the orbitals used in this study. The $1\pi_g$ state is well resolved, whereas the $4\sigma_g$ state is resolved sufficiently to ensure accurate cross-section measurements can be obtained. For details, see text.

data accumulation the vacuum pressure was maintained at 1×10^{-5} Torr, as measured by a Varian UHV-24 ion gauge located ~ 50 cm from the interaction region. Incident electron beam currents between 40 nA and 200 nA were adopted with data collection times from 1000 to 4000 s for each coincidence measurement. Drifts in the spectrometer tuning were minimized by the use of a computer control and optimization technique [2, 19]. The DCS measurements for a given energy and orbital were averaged over a number of sweeps of the detection plane, the associated error for each final data point being the standard deviation from this average. True coincidence count rates ranged between $\sim$0.2 Hz and 2 Hz, and the collection time for a particular valence orbital and energy ranged between one and two weeks.

The incident electron energy was calibrated by measuring the ionization coincidence signal from CO_2, figure 2 illustrating the coincidence binding energy spectrum obtained. The spectrum was collected in a coplanar symmetric geometry where the outgoing electrons were detected with fixed equal energies $E_a = E_b = 20$ eV and at equal scattering angles $\xi = 50^\circ$. The data are averaged over three sweeps of the incident electron energy between 50 eV and 60 eV using an energy interval of 0.2 eV. The associated error on each data point is the standard deviation of the average from these runs. The spectrum has been corrected for a contact potential of $\sim$1.05 eV, as determined by comparison with published ionization potentials for CO_2 [20].

The binding energy spectrum shown in figure 2 is qualitatively similar to that obtained in non-coplanar electron momentum spectroscopy studies [21–24] and in photo-ionization studies [25]. The $1\pi_g$ and $4\sigma_g$ orbitals are clearly observed at binding energies of 13.77 eV and 19.39 eV, respectively. By contrast, the $1\pi_u$ and $3\sigma_u$ orbitals with respective ionization potentials of 17.31 eV and 18.07 eV were not resolved and appear as a single peak centred at $\sim$18 eV. As these were not resolved, DCS measurements from these orbitals were not taken, and so the measurements presented here are only from the $1\pi_g$ and $4\sigma_g$ orbitals. Although the binding energy of the $4\sigma_g$ orbital is close to the energy of the combined $1\pi_u$ and $3\sigma_u$ states,

Gaussian functions fitted to the binding energy spectrum indicate that the contribution to the $4\sigma_g$ cross section from these states is minimal, as shown in figure 2.

As an additional check on the angular calibration of the spectrometer, a survey of the DCS for ionization of the 1s atomic orbital of He in this energy range was conducted. The results were in agreement with previous measurements by the Manchester and Kaiserslautern groups [4, 26].

3. Results and discussion

The ground-state electronic configuration of the linear tri-atomic molecule CO_2 is given by:

$$(1\sigma_u)^2(1\sigma_g)^2(2\sigma_g)^2(3\sigma_g)^2(2\sigma_u)^2(4\sigma_g)^2(3\sigma_u)^2(1\pi_u)^4(1\pi_g)^4X^1\Sigma_g^+ \quad (3)$$

where the ionization potentials of the outer $1\pi_g$, $1\pi_u$, $3\sigma_u$ and $4\sigma_g$ orbitals are 13.77 eV, 17.31 eV, 18.07 eV and 19.39 eV, respectively. Ionization from these outer orbitals produces the $X^2\Pi_g$, $A^2\Pi_u$, $B^2\Sigma_u^+$ and $C^2\Sigma_g^+$ states of the ion, respectively. The results presented here are DCS measurements for ionization from the $1\pi_g$ valence orbital and $4\sigma_g$ inner-valence orbital. The absence of an accurate theoretical model to describe electron impact ionization of molecules at incident energies below 100 eV, particularly for coplanar symmetric studies, limits the discussion to a qualitative comparison with previous low energy coplanar symmetric studies.

3.1. Ionization from the $1\pi_g$ orbital of CO_2

Figures 3(a)–(e) show the DCS measurements for ionization from the $1\pi_g$ orbital at incident energies $E_0 = 23.8$ eV, 33.8 eV, 43.8 eV, 53.8 eV and 73.8 eV, corresponding to $E_a = E_b =$ 5 eV, 10 eV, 15 eV, 20 eV and 30 eV, respectively. The measurements were collected between $\xi = 40^\circ$ and $\xi = 125^\circ$ at intervals of 5°, the results at $E_0 = 33.8$ eV also including data at $\xi =$ 35°. The larger angular range at this energy was possible due to removal of the TOFMS as discussed above. To permit comparison between measurements, the results are presented on the same linear scale. Since the experiment did not measure absolute cross sections, all measurements are normalized to unity at $\xi = 45^\circ$. The error bars represent the statistical variation of the data accumulated over 15–20 sweeps of the detection plane.

From these data it is clear that the DCS peaks in a forward direction for all energies, and that this 'binary' peak shifts in position to smaller angles as the energy increases. In a simple approximation, this binary feature may be attributed to a single collision between the incident and bound electrons. At $E_a = E_b = 5$ eV, the forward peak occurs at an angle $\xi \sim 70^\circ$. As the energy increases the position of the peak moves until at $E_a = E_b = 30$ eV the peak position occurs at an angle lower than measured by the spectrometer. In a similar way, the position of the minimum ($\xi \sim 105^\circ$ at $E_a = E_b = 5$ eV) also decreases in angle as the energy increases, although at a slower rate. The minimum is also seen to broaden as the energy increases.

The data indicate that significant cross section also occurs in the backscatter region ($\xi > 125^\circ$) at all measured energies, although the relative intensity and position of the backscatter peak cannot be determined accurately since it lies beyond the angular range of these measurements. There appears to be an additional small feature occurring at $\xi \sim 70^\circ$ which is most obvious at $E_a = E_b = 20$ eV, but which can also be seen at lower energies. This feature has apparently disappeared for $E_a = E_b = 30$ eV. Since the initial target state is a π state, this feature may be a signature of the momentum distribution of a bound electron with $\lambda = 1$, where λ is the quantum number for the projection of the electron's orbital angular momentum onto the inter-nuclear axis of the molecule, as observed in low energy coplanar symmetric studies of ionization from atoms such as argon [27] and neon [28].

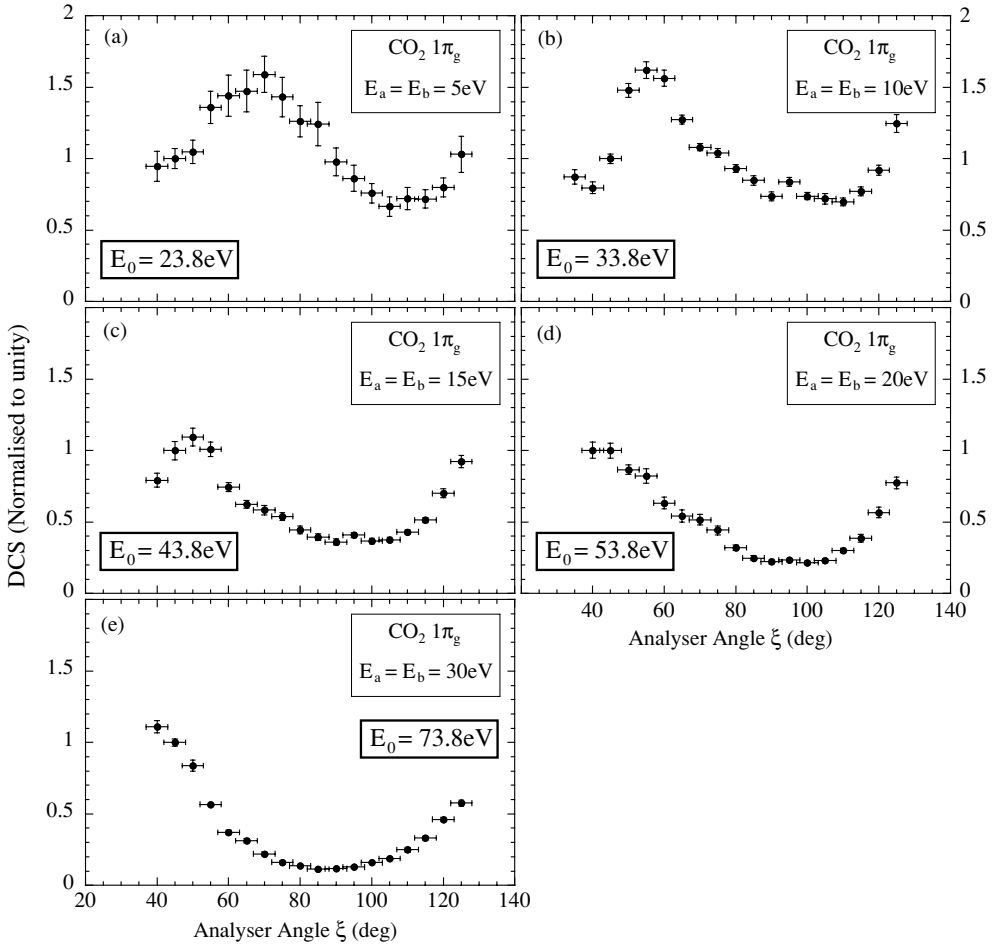

Figure 3. Differential cross section results from the $1\pi_g$ state of CO_2, for $E_a = E_b =$ (a) 5 eV, (b) 10 eV, (c) 15 eV, (d) 20 eV and (e) 30 eV. The results are normalized to unity at $\xi = 45^\circ$.

The results from CO_2 are compared to those from the $1\pi_u$ state of N_2, which are reproduced from [7] in figure 4. In the N_2 results the energy of the outgoing electrons again ranges from 5 eV through to 30 eV. The results are placed on a linear scale and are again normalized to unity at $\xi = 45^\circ$.

Although similarities can be seen between the results for N_2 and CO_2, there are clear differences which must arise due to differences in the targets. By contrast with CO_2, at $E_a = E_b = 5$ eV the results from N_2 show a forward peak at $\xi \sim 60^\circ$, which moves to $\xi \sim 40^\circ$ at $E_a = E_b = 10$ eV and remains in this position at higher energies. The minimum at $E_a = E_b = 5$ eV is at $\xi \sim 115^\circ$, and this minimum moves to lower angles as the energy increases, as also observed for CO_2. At $E_a = E_b = 30$ eV the minimum is broadened as also seen in CO_2.

The backscatter peak is once more found beyond the measurable range for N_2 at all energies, however unlike CO_2 the backscatter signal is smallest when $E_a = E_b = 5$ eV, increases to a maximum when $E_a = E_b = 20$ eV and then reduces significantly when $E_a = E_b = 30$ eV. There is a clear feature at $\xi \sim 70^\circ$ for $E_a = E_b = 10$ eV, which Hussey and Murray [7] again suggest is due to the momentum distribution of the bound π electron with $\lambda = 1$.

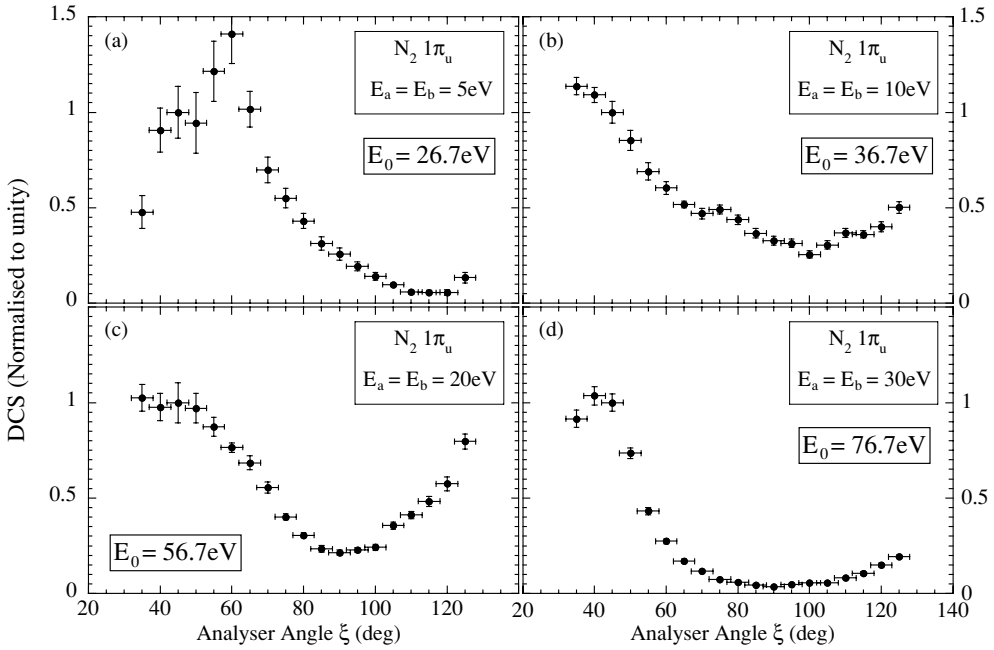

Figure 4. Differential cross section results from the $1\pi_u$ state of N_2, for $E_a = E_b =$ (a) 5 eV, (b) 10 eV, (c) 20 eV and (d) 30 eV. The results are normalized to unity at $\xi = 45^\circ$.

Table 1. DCS results from the $1\pi_g$ state of CO_2 and the $1\pi_u$ state of N_2 normalized to unity at $\xi = 45^\circ$, showing the position and relative intensities of the maxima and minima in the measured cross section.

	CO_2					N_2			
$E_a = E_b =$	5 eV	10 eV	15 eV	20 eV	30 eV	5 eV	10 eV	20 eV	30 eV
Forward peak position	70°	55°	50°	~43°	<40°	60°	~35°	~40°	40°
Forward peak height	1.59 ± 0.13	1.62 ± 0.06	1.10 ± 0.06	1.00 ± 0.05	1.11 ± 0.04	1.41 ± 0.15	1.13 ± 0.04	1.00 ± 0.11	1.04 ± 0.05
Position of minimum	105°	~103°	100°	95°	85°	115°	100°	90°	90°
DCS minimum	0.67 ± 0.07	0.69 ± 0.03	0.37 ± 0.02	0.22 ± 0.01	0.11 ± 0.01	0.06 ± 0.01	0.26 ± 0.02	0.21 ± 0.01	0.04 ± 0.01
DCS ($\xi = 125^\circ$)	1.03 ± 0.13	1.25 ± 0.06	0.92 ± 0.04	0.77 ± 0.04	0.58 ± 0.02	0.13 ± 0.03	0.50 ± 0.03	0.80 ± 0.04	0.19 ± 0.01

Table 1 summarizes these results for both CO_2 and N_2 to enable numerical comparison between the different targets.

It was suggested in [7] that for N_2, the movement in the forward peak towards $\xi = 90^\circ$ as the energy of the outgoing electrons reduces to 5 eV may be due to post-collisional interactions (PCI) between the outgoing electrons following the interaction, as observed in helium at similar low energies [18]. It is unlikely that PCI is the main cause of the shift in the forward peak position in CO_2 as given in table 1, as the peak continuously moves to lower angles as the energy increases to $E_a = E_b = 30$ eV, where PCI will not play a significant role. A further indication that PCI is not dominating the interaction when $E_a = E_b = 5$ eV is that the backscatter peak would also move towards $\xi = 90^\circ$, and there is no evidence that this is occurring. Other mechanisms must, therefore, be causing the change in position of the forward scatter peak.

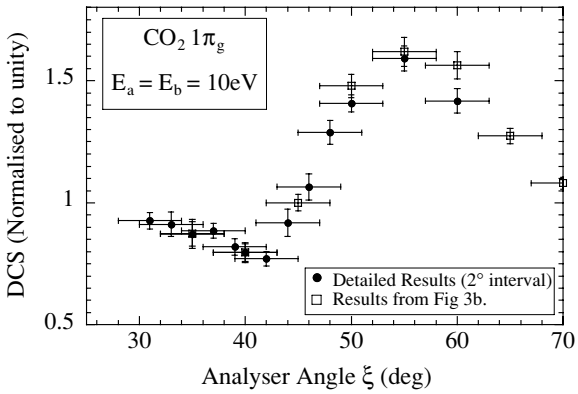

Figure 5. DCS measurements from the $1\pi_g$ state of CO_2 for $E_a = E_b = 10$ eV, using an angular variation of 2° from $\xi = 31°$ to $\xi = 50°$. A new minimum is found at $\xi \sim 42°$, with a second forward maximum at $\xi \sim 30°$. The results are again normalized to unity at $\xi = 45°$.

3.2. Measurements from the $1\pi_g$ orbital of CO_2 when $E_a = E_b = 10$ eV

Closer analysis of the results in figure 3(b) where $E_a = E_b = 10$ eV shows an *increase* in the cross section at $\xi = 35°$ compared to that at $\xi = 40°$. This is a surprising result, as the DCS in a coplanar symmetric geometry must reduce to zero when $\xi = 0°$ and 180°. This increase was observed consistently in the data for each sweep of the detection plane, and so it was decided to investigate this more closely. To facilitate this, the analyser positions were carefully checked to establish minimum safe working angles before they collided with the Faraday cup used to collect un-scattered electrons in the electron beam (see figure 1). The minimum angle which could be used was $\xi = 31°$, so a detailed set of data was taken every 2° from $\xi = 31°$ to $\xi = 50°$ at this energy.

The results of these studies are shown in figure 5, superimposed on the data from figure 3(b). There is excellent agreement between the two data sets for $\xi \geqslant 35°$, both being normalized to unity at $\xi = 45°$. The more detailed data at lower scattering angles show that the DCS has a local minimum at $\xi \sim 42°$, and that for angles less than 42° the cross section once more *increases*. The results indicate that a local maximum occurs around $\xi = 30°$. It would clearly be beneficial to take data at lower scattering angles to define the cross section more fully, and we are presently considering techniques to modify the (e, 2e) spectrometer at Manchester to allow this.

A secondary maximum at low-scattering angles has also been observed in the DCS for ionization of targets including CO, Ar and Ne. Rioual *et al* [8] observed a double maximum in the region $\xi < 60°$ for ionization of the 1π orbital of CO using an incident electron energy $E_0 = 400$ eV. A similar structure is also apparent in the results of Rouvellou *et al* [29], Murray *et al* [27], Bell *et al* [30] for ionization of the 3p orbital of Ar, and Murray and Read [28] for the 2p orbital of Ne, although none of the results show as clear a minimum as seen here. These authors attribute the local minimum in the cross section at small angles to the momentum of the bound valence p-electron. The similarity of the low angle results for ionization of the $1\pi_g$ orbital of CO_2 presented here (and for the 1π orbital of CO in [8]) with the atomic results for ionization of Ar [27, 29, 30] may imply that the atomic p-state origin of the π-orbital is an important factor in determining the ionization cross section. It will be interesting to see if theoretical models of the interaction can provide further information as to the cause of this feature.

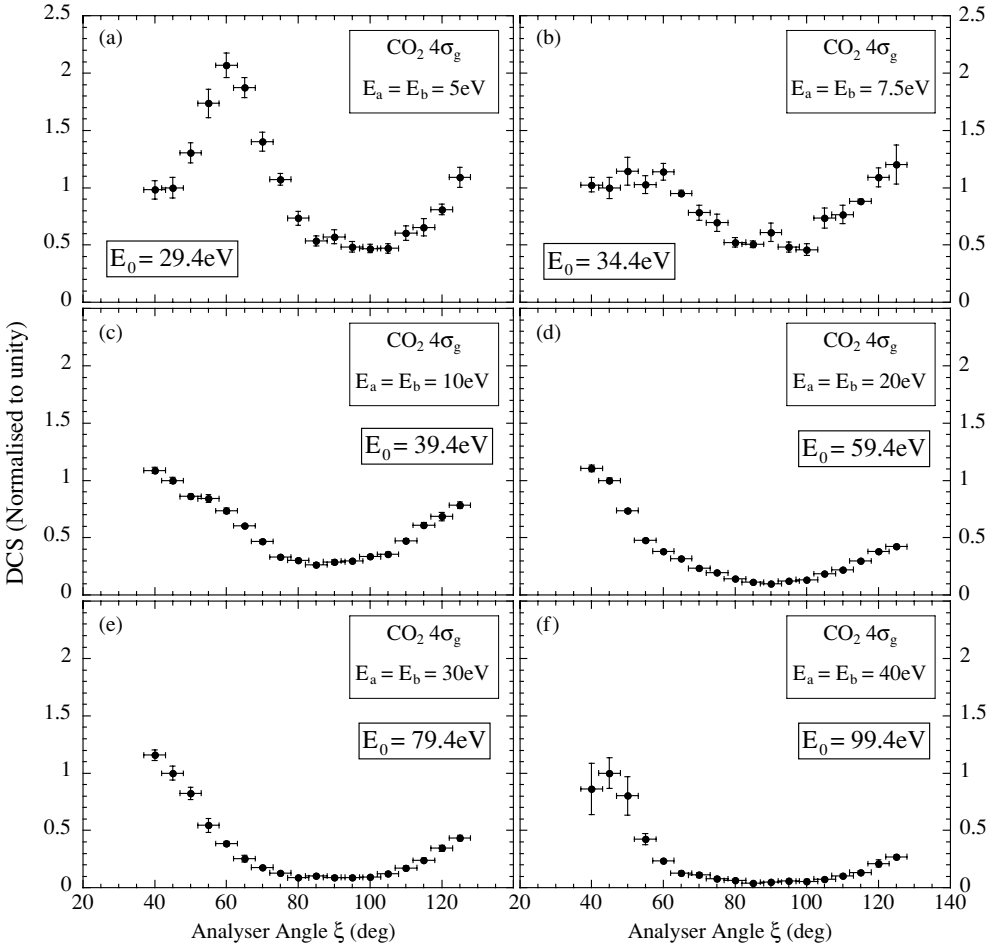

Figure 6. Differential cross section results from the $4\sigma_g$ state of CO_2, for $E_a = E_b =$ (a) 5 eV, (b) 7.5 eV, (c) 10 eV, (d) 20 eV, (e) 30 eV and (f) 40 eV. The results are normalized to unity at $\xi = 45^\circ$.

3.3. Measurements from the $4\sigma_g$ orbital of CO_2

Ionization measurements from the $4\sigma_g$ state of CO_2 were also conducted over a range of energies, since the $4\sigma_g$ state could be separated from the unresolved $1\pi_u$ and $3\sigma_u$ states around 18 eV as shown in figure 2. Six sets of results were obtained from 10 eV to 80 eV above the ionization threshold, for outgoing electron energies of 5 eV, 7.5 eV, 10 eV, 20 eV, 30 eV and 40 eV. The data were again normalized to unity at $\xi = 45^\circ$.

Figure 6 shows the data that were obtained, presented on a linear scale. At $E_a = E_b = 5$ eV, there is a clear forward peak at $\xi = 60^\circ$, the minimum in the cross section occurring at $\xi \sim 100^\circ$. The backscatter peak occurs at an angle $\xi > 125^\circ$. As the energy increases, the forward peak is again seen to move towards lower scattering angles, and the minimum in the cross section moves slowly towards $\xi \sim 85^\circ$ when $E_a = E_b = 40$ eV. At the highest energy the forward peak position appears to be around $\xi = 45^\circ$, although the uncertainty in the measurements does not allow a definite conclusion to be reached. At all energies the backscatter peak occurs beyond

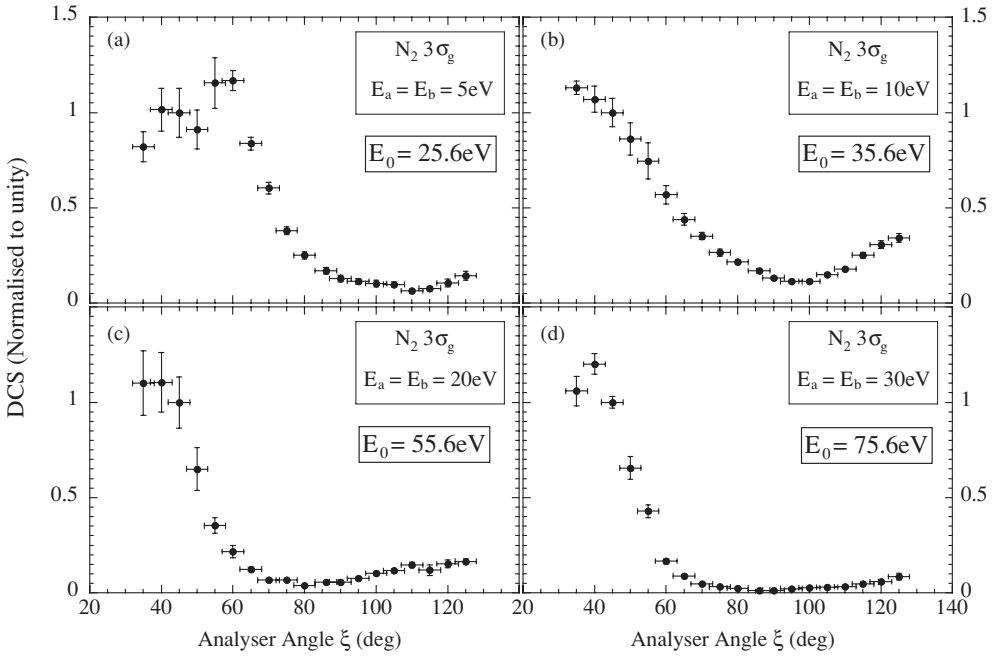

Figure 7. Differential cross section results from the $3\sigma_g$ state of N_2, for $E_a = E_b =$ (a) 5 eV, (b) 10 eV, (c) 20 eV and (d) 30 eV. The results are normalized to unity at $\xi = 45^\circ$.

Table 2. DCS results from the $4\sigma_g$ state of CO_2 and the $3\sigma_g$ state of N_2 normalized to unity at $\xi = 45^\circ$, showing the position and relative intensities of the maxima and minima in the measured cross section.

	CO_2					N_2				
$E_a = E_b =$	5 eV	7.5 eV	10 eV	20 eV	30 eV	40 eV	5 eV	10 eV	20 eV	30 eV
Forward peak position	60°	50°	<40°	<40°	<40°	~45°	~50°	~35°	40°	40°
Forward peak height	2.07 ± 0.11	1.14 ± 0.07	1.09 ± 0.03	1.10 ± 0.03	1.15 ± 0.04	1.00 ± 0.13	1.16 ± 0.05	1.13 ± 0.04	1.11 ± 0.16	1.20 ± 0.05
Position of minimum	100°	95°	85°	90°	90°	~85°	110°	95°	80°	85°
DCS minimum	0.47 ± 0.04	0.46 ± 0.05	0.27 ± 0.02	0.10 ± 0.01	0.09 ± 0.01	0.04 ± 0.01	0.06 ± 0.01	0.11 ± 0.01	0.04 ± 0.01	0.01 ± 0.01
DCS ($\xi = 125^\circ$)	1.09 ± 0.09	1.20 ± 0.17	0.78 ± 0.03	0.42 ± 0.02	0.44 ± 0.03	0.27 ± 0.02	0.14 ± 0.02	0.34 ± 0.02	0.17 ± 0.01	0.09 ± 0.02

the measurable range at $\xi > 125^\circ$, however the relative magnitude of the DCS seems to decrease relatively uniformly as the energy increases, unlike the results from the $1\pi_g$ state.

As above, these results are compared to the measurements from the $3\sigma_g$ state of N_2 [7], which are presented in figure 7 on a linear scale. Clear differences are again seen between the two targets. At $E_a = E_b = 5$ eV, the results from the $3\sigma_g$ state of N_2 show a forward scattering peak at $\xi \sim 50^\circ$, and a very small contribution in the backscatter region. The forward peak in N_2 appears to remain around $\xi \sim 40^\circ$ as the energy increases, and is the dominant feature at all energies. When $E_a = E_b = 10$ eV the backscatter peak is a maximum, whereas at higher energies this decreases in magnitude significantly. In all cases, the backscatter peak occurs at $\xi > 125^\circ$. The minimum in the cross section again moves to lower scattering angles as the energy increases, which is in common with all results from both CO_2 and N_2.

Table 2 summarizes these results for both CO_2 and N_2 to again enable numerical comparison between the different targets.

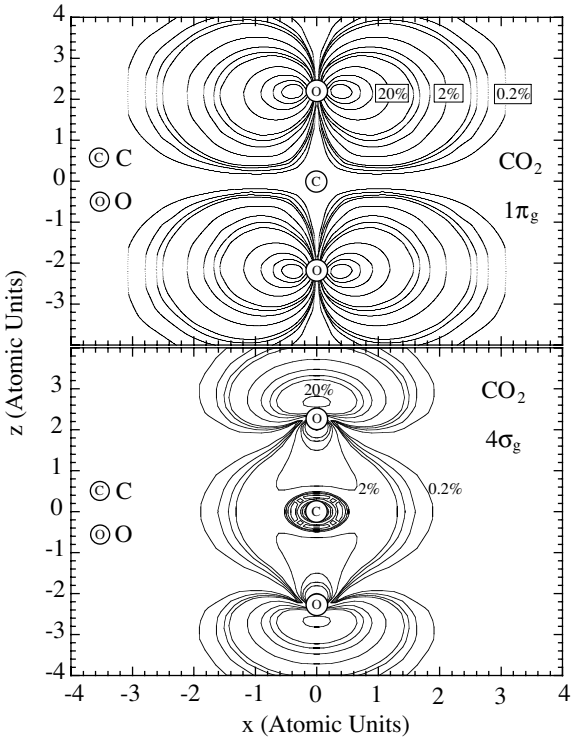

Figure 8. Electron charge densities for the $1\pi_g$ and $4\sigma_g$ states of CO_2 reproduced from the data of Chen *et al* [22]. The position of the carbon and oxygen nuclei are shown. The contours indicate the probability of finding the electrons as 0.2%, 0.4%, 0.6%, 0.8%, 2%, 4%, 6%, 8%, 20%, 40%, 60% and 80%.

One of the main differences between the $1\pi_g$ and $4\sigma_g$ states of CO_2 can be seen in the electron charge cloud density distribution around the nuclei, as reproduced in figure 8 from the data of Chen *et al* [22]. The $1\pi_g$ state is seen to be a repulsive state, with the electron charge density predominantly surrounding the two oxygen atoms in the linear molecule. There is almost zero probability of finding the electron near the carbon atom, and so the interaction between the incident electron and bound electrons in this state should approximate a region with two scattering centres, whereas interaction with the carbon and oxygen nuclei will be from three distinct scattering centres.

The absence of electron charge density around the carbon atom may be the cause of the unusual forward peak observed at $\xi \sim 30^\circ$ when $E_a = E_b = 10$ eV, however without theoretical input this can only be speculation.

By contrast, the electron charge density for the $4\sigma_g$ state is seen to be very different. In this state the electrons have the highest probability of occupying a region close to the carbon atom, and have only ∼20% probability of being near the two oxygen atoms. The target, therefore, has three regions where electron–electron interactions are likely, in contrast to the $1\pi_g$ state with two.

The spatial extent of the $4\sigma_g$ state is seen to be smaller than the $1\pi_g$ state, which is reflected in the higher binding energy of this state (figure 2). The proximity of the electrons to the ion core will partly shield the core from the incident electron. This may explain why scattering in the backward direction is less probable for this state compared to the $1\pi_g$ state,

where the incident electron is expected to be influenced by the ion core over a larger region of space.

Clearly, for a detailed calculation of the ionization process *all* bound electrons must be considered in the scattering process. In particular for the inner-valence $4\sigma_g$ orbital, eight electrons occupy the outer-valence $1\pi_u$ and $1\pi_g$ orbitals, all of which have lower binding energy than electrons in the $4\sigma_g$ orbital. These outer electrons are likely to influence ionization from the $4\sigma_g$ orbital in a dynamic way, and so models which average over the position of these non-ionized electrons will probably prove to be inaccurate.

4. Summary and conclusions

In this paper new results for ionization of the tri-atomic molecule CO_2 have been presented. The measurements were conducted in a coplanar symmetric geometry at low incident energies. The results have been compared to those obtained from diatomic N_2 collected using the same spectrometer, the character of the states in each molecule (π and σ states) being the same. Clear differences are observed, which must be due to differences between the target configurations.

An unusual feature has been seen at low incident energy for ionization from the $1\pi_g$ state of CO_2, the cross section having a local minimum in the forward direction at around 42°, with a further maximum around 30°. Similar structures reported for targets including CO, Ar and Ne have been tentatively attributed to the momentum of the bound p-electron. The feature seen here may, therefore, imply that the p-state origin of the π-orbital is an important factor determining the ionization cross section. Further experiments are required to fully detail this structure.

The results presented here will hopefully promote theoretical interest in ionization from molecules at low to intermediate energies. Although this region is the most difficult to model, it is here that the ionization cross section is highest. It is, therefore, essential that accurate models are developed in this region, and the experimental results in this paper should provide a good basis for new developments in this area.

Acknowledgments

We would like to thank the Engineering and Physical Science Research Council in the United Kingdom for supporting this work, and for providing a research studentship (MJH). We would also like to thank Alan Venables and Dave Coleman for providing continual excellent technical support during the building phase of this project.

References

[1] McCarthy I E and Weigold E 1995 *Electron–Atom Collisions* (Cambridge: Cambridge University Press)
[2] Murray A J, Turton B C and Read F H 1992 *Rev. Sci. Instrum.* **63** 3346–51
[3] Murray A J and Read F H 1993 *Phys. Rev.* A **47** 3724
[4] Murray A J and Read F H 1992 *Phys. Rev. Lett.* **69** 2912
[5] Röder J, Erhardt H, Bray I, Fursa D V and McCarthy I E 1996 *J. Phys. B: At. Mol. Opt. Phys.* **29** 2103
[6] Whelan C T, Walters H R, Allan R J and Zhang X 1993 *(e, 2e) and Related Processes* (Dordrecht: Kluwer) p1
[7] Hussey M J and Murray A J 2002 *J. Phys. B: At. Mol. Opt. Phys.* **35** 3399–409
[8] Rioual S, Nguyen V G and Pochat A 1996 *Phys. Rev.* A **54** 4968
[9] Cavanagh S J and Lohmann B 1999 *J. Phys. B: At. Mol. Opt. Phys.* **32** L261
[10] Avaldi L and Camilloni R 1990 *Phys. Rev.* A **41** 134
[11] Milne-Brownlie D S, Cavanagh S J, Lohmann B, Champion C, Hervieux P A and Hanssen J 2004 *J. Phys. Rev.* A **69** 032701

[12] Stia C R, Fojón O A, Weck P F, Hanssen J and Rivarola R D 2002 *Phys. Rev.* A **66** 052709
[13] Gao J, Madison D H and Peacher J L 2005 Private communication
[14] Avaldi L, Camilloni R, Fainelli E and Stefani G 1992 *J. Phys. B: At. Mol. Opt. Phys.* **25** 3551
[15] Haynes M A and Lohmann B 2003 *J. Phys. B: At. Mol. Opt. Phys.* **36** 811
[16] Haynes M A and Lohmann B 2001 *J. Phys. B: At. Mol. Opt. Phys.* **34** L131
[17] Murray A J and Read F H 2001 *Phys. Rev.* A **63** 0127141
[18] Bowring N J, Murray A J and Read F H 1997 *J. Phys B: At. Mol. Opt. Phys.* **30** L671
[19] Hussey M J 2003 *PhD Thesis* The Victoria University of Manchester
[20] Berkowitz J 1979 *Photoabsorption, Photoionization & Photoelectron Spectroscopy* (New York: Academic)
[21] Brion C E and Tan K H 1978 *Chem. Phys.* **34** 141
[22] Chen X J, Ouyang G, Jia C C, Peng L L, Xu C K, Tian S X and Xu K Z 2000 *J. Electron Spectrosc. Relat. Phenom.* **107** 273
[23] Cook J P D and Brion C E 1982 *Chem. Phys.* **69** 339
[24] Giardini-Guidoni A, Tiribelli R, Vinciguerra D, Camilloni R and Stefani G 1977 *J. Electron Spectrosc. Relat. Phenom.* **12** 405
[25] Gustafsson T, Plummer E W, Eastman D E and Gudat W 1978 *Phys. Rev.* A **17** 175
[26] Rosel T, Dupre C, Röder J, Duguet A Jung K, Lahmam-Bennani A and Ehrhardt H 1991 *J. Phys. B: At. Mol. Opt. Phys.* **24** 3059
[27] Murray A J, Bowring N J and Read F H 2000 *J. Phys. B: At. Mol. Opt. Phys.* **33** 2859
[28] Murray A J and Read F H 2000 *J. Phys. B: At. Mol. Opt. Phys.* **33** L297
[29] Rouvellou B, Rioual S, Röder J, Pochat A, Rasch J, Whelan C T, Walters H R J and Allan R J 1998 *Phys. Rev.* A **57** 3621
[30] Bell S, Gibson C T and Lohmann B 1995 *Phys. Rev.* A **51** 2623